Optical and near-IR spectrophotometry of the galaxy NGC 3310

Miriani G. Pastoriza,[1] Horacio A. Dottori,[1] Elena Terlevich,[2] Roberto Terlevich[2] and Angeles I. Díaz[3]

[1] *Depto de Astronomia, Instituto de Física – UFRGS, CP 15051, Porto Alegre, 91500, RS, Brazil*
[2] *Royal Greenwich Observatory, Madingley Road, Cambridge CB3 0EZ*
[3] *Depto de Física Teórica, C-XI, Universidad Autónoma de Madrid, Cantoblanco, 28049-Madrid, Spain*

ABSTRACT
We present spectrophotometric observations in the optical and near-infrared of the nucleus and six H II regions in the spiral galaxy NGC 3310. Four of the regions are circumnuclear at less than 400 pc from the nucleus, and two are located in the spiral arms at 600 and 1600 pc respectively. Abundance analysis complemented with detailed photoionization models indicates that, while the circumnuclear and disc H II regions have a moderately low metallicity (0.2–0.4 $Z_\odot$), the nucleus has solar abundances. No radial gradient was detected away from the nuclear region. The IR Ca II triplet in absorption is observed in some of the H II regions and a moderately strong WR spectral feature at 4686 Å in the brightest H II region 9 arcsec SW of the nucleus is also reported. The simultaneous occurrence of these features in H II regions with strong emission lines indicates that star formation lasted a few million years.

Key words: H II regions – galaxies: abundances – galaxies: individual: NGC 3310 – galaxies: peculiar – galaxies: stellar content.

1 INTRODUCTION

The possible connection between nuclear activity and star formation has recently received considerable attention and there is a rapidly growing body of evidence suggesting a link, possibly evolutionary, between AGN and starbursts (Terlevich & Melnick 1985; Terlevich, Melnick & Moles 1987; Norman & Scoville 1988). Several so-called hotspot galaxies are composite in nature with a central LINER or Seyfert-like nucleus surrounded by star-forming regions. The central hotspots have high surface brightness, being comparable in luminosity to bright giant H II regions. Their most unusual property is a very strong optical continuum relative to the emission-line luminosity. This may reflect a long history of star formation or, alternatively, an unusual stellar mass spectrum in the ionizing cluster (Kennicutt, Keel & Blaha 1989: KKB). In order to understand the properties of nuclear and extranuclear bursts of star formation, we have embarked on a detailed study of nearby hotspot galaxies of which NGC 3310 is one of the most outstanding examples.

NGC 3310 has been classified as an SAB(r)bc peculiar galaxy of luminosity class II (de Vaucouleurs, de Vaucouleurs & Corwin 1976). The central part of the galaxy shows a conspicuous 20-arcsec diameter ring of luminous giant H II regions surrounding the blue compact nucleus. This corre-

sponds to ~1.2 kpc at the adopted distance of 12.5 Mpc (Bottinelli et al. 1984). This distinctive feature led Sersic & Pastoriza (1967) to classify it as a hotspot galaxy. NGC 3310 is included in the catalogue of interacting galaxies (Vorontsov-Velyaminov 1977) and in Arp's (1966) Atlas of Peculiar Galaxies.

The giant H II regions in the ring have been found to be more luminous than average giant H II regions, and of low metallicity compared to the inner regions of galaxies with similar Hubble type and luminosity (Heckman & Balick 1980). The velocity field shows non-circular streaming motions and the dynamical centre seems to be displaced from the nucleus (van der Kruit 1976). The rotation curve near the centre is one of the steepest found among spiral galaxies, giving a central mass of 1×10^9 $M_\odot$ (Grothues & Schmidt-Kaler 1991: GSK91). Another distinctive feature is the presence of a chain of bright knots at about 1 arcmin to the north-west of the nucleus at PA ~300°, interpreted by Bertola & Sharp (1984) as a jet formed in an explosive event some 1.8×10^7 yr ago.

Infrared 10-µm and *JHKL* colours indicate that the blue *UBV* colours and intense radio, ultraviolet and X-ray emission detected in this galaxy can be attributed to a luminous burst of star formation younger than 10^7 yr (Telesco & Gatley 1984). Strong near-IR Ca II absorption

lines, signature of young red supergiants, have been reported in one of the circumnuclear giant H II regions (Terlevich et al. 1990).

Radio continuum maps show strong radio sources coincident with the giant H II regions localized in the inner ring and the arms of the galaxy (van der Kruit & de Bruyn 1976; Seaquist & Bignell 1977). The radio emission seems to be stronger than that of a normal spiral.

We have obtained high-quality spatially resolved spectrophotometric data over a wide spectral range (3600–9600 Å) which allow us to study the ionization structure of the inner 20 arcsec of NGC 3310 and to deduce the abundances of the most important elements (O, S, N, Ne and He) as well as the properties of the ionizing star clusters (age, metallicity, number of ionizing stars, etc.).

We present the observations and data reduction in Section 2 and the data analysis in Section 3. The H II region parameters are presented in Section 4. In Section 5 we discuss the WR features in the most luminous H II region and in Section 6 we model the ionizing stellar associations. Finally, the discussion and main conclusions are presented in Section 7.

2   OBSERVATIONS AND DATA REDUCTION

The data were obtained in 1989 March with the Isaac Newton Telescope (INT) at the Roque de Los Muchachos Observatory using the intermediate dispersion spectrograph (IDS), the 235-mm camera and a blue coated GEC CCD. Two different gratings were used (both with 400 groove mm^{-1}) to cover a total spectral range from 3650–9700 Å in five individual spectra of about 1400 Å each. The dispersion of 2.3 Å per pixel with the slit width used for the observations (1.5 arcsec) yields a spectral resolution of about 4 Å. The size of the CCD along the spatial direction is 400 pixels of 0.7 arcsec. The slit was set in three different positions over the central region of the galaxy at PA 347°, 347° (10 arcsec off nucleus) and 317°, which are marked in the Hα image of Fig. 1, and called position 1, 2 and 3 respectively in the journal of observations (Table 1).

The data reduction was performed with the IRAF package at IF–UFRGS following standard procedures. The CCD frames were dark current bias subtracted and flat-fielded. The subsequent steps in the reduction were sky subtraction, extinction correction and flux calibration. Sets of increments compressed to one dimension were chosen on the basis of the spatial light distribution along the slit for the different position angles. Since the nebular emission is extended and filled most of the slit, sky subtraction was performed using the outermost increments in every data frame. The spectra were corrected for continuous atmospheric extinction using an extinction curve appropriate for La Palma Observatory. The atmospheric absorption bands present in the infrared
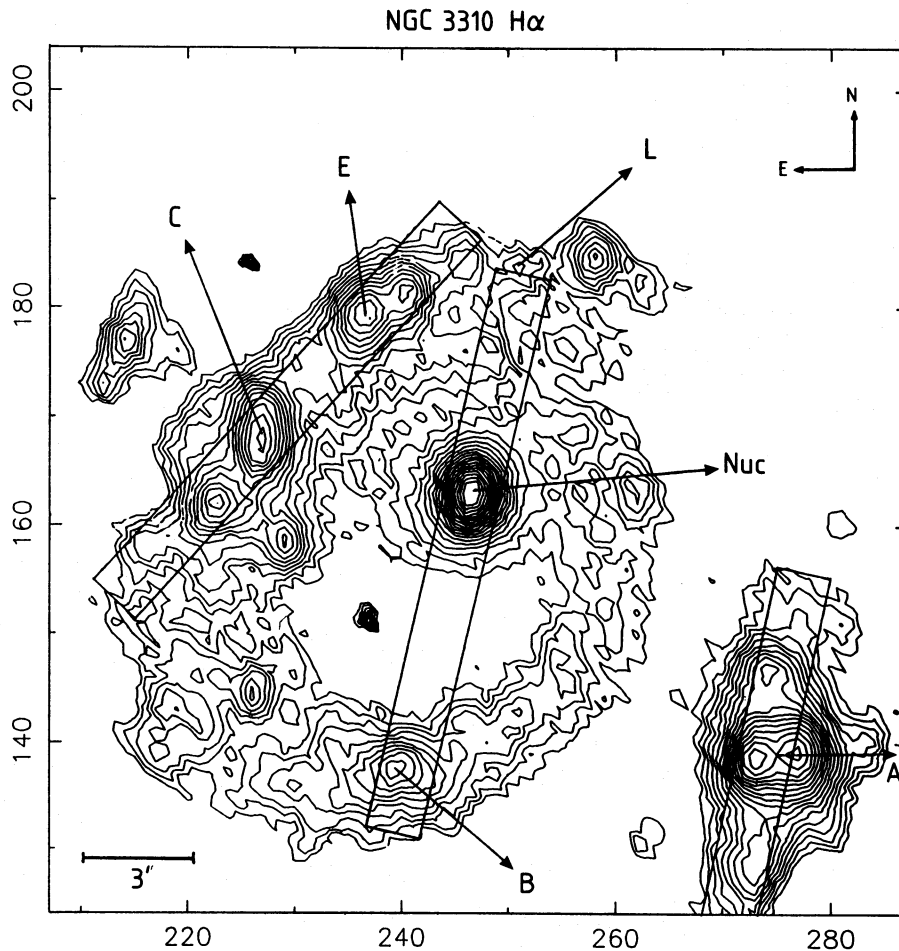

Figure 1. Hα image of NGC 3310 showing our selected slit positions. Nuc, A, B, C, E and L label the regions studied in the abundance analysis.

Table 1. Journal of observations.

Position	Night	P.A.	Grating	$\Delta\lambda$ (Å)	Exposure (s)
1	March 20/21	347	400V	4759-6076	1300
1	March 20/21	347	400V	4759-6079	1300
1	March 20/21	347	400V	3581-4953	1800
1	March 20/21	347	400V	3581-4953	1800
1	March 20/21	347	400V	5942-7265	1000
1	March 20/21	347	400V	5942-7265	1000
1	March 20/21	347	400R	7163-8490	1300
1	March 20/21	347	400R	7163-8490	1300
1	March 20/21	347	400R	8359-9691	1800
2	March 21/22	347Off	400V	4759-6076	1300
2	March 21/22	347Off	400V	4759-6076	1300
2	March 21/22	347Off	400V	3581-4953	1800
2	March 21/22	347Off	400V	3581-4953	1800
2	March 21/22	347Off	400V	5942-7265	1300
2	March 21/22	347Off	400V	5942-7265	1300
2	March 21/22	347Off	400R	8359-9691	1800
2	March 21/22	347Off	400R	8359-9691	1100
2	March 21/22	347Off	400R	7163-8490	1300
3	March 21/22	317	400V	4759-6076	1300
3	March 21/22	317	400V	4759-6076	1300
3	March 21/22	317	400V	3581-4953	1800
3	March 21/22	317	400V	3581-4953	1800
3	March 22/23	317	400R	8359-9691	1800
3	March 22/23	317	400R	8359-9691	1800
3	March 22/23	317	400R	5942-7265	1000
3	March 22/23	317	400R	5942-7265	1000
3	March 22/23	317	400R	7163-8490	1300

part of the spectrum have been removed by means of division star (HD 140283) following the procedure described in Díaz, Pagel & Wilson (1985). Oke & Gunn (1983) standards HD 84937, HD 102224 and HD 140283 were used for flux calibration.

3 DATA ANALYSIS

The spatial distribution of the more relevant emission lines along the slit for the three position angles observed is illustrated in Figs 2-4. These show the structure of the inner region of the galaxy and were used to define the regions from which the spectra have been extracted. These regions are also indicated in Fig. 1. The merged spectra for the nucleus and the circumnuclear H II regions B, C, E and L are presented in Figs 5(a)-(e). The figures are plotted with two intensity scales in order to show the weakest lines. The merged spectrum of the off-nuclear giant H II region A (hereafter 'Jumbo') is shown in Fig. 5(f). Note the broad WR feature seen from 4400 to 4700 Å. An enlargement of this part of the spectrum is presented in Fig. 5(g). The most prominent lines have been preliminarily identified as N III, N V, [Fe III], He I, He II and [Ar IV]. We will discuss these features in detail in Section 5.

3.1 Spatial profiles of the emission lines

An idea of the spatial behaviour of the emission-line intensity ratios [O II]3727/[O III]5007, [S II]6717, 6730/[S III]9532 and [N II]6583/Hα can be obtained from the profiles presented in Figs 2-4, where the corresponding pairs have been plotted

together for the three slit positions. Due to the wavelength range covered by the line pairs, except for [N II] and Hα, these profiles do not represent real excitation differences, as they are affected by reddening.

The ratio [N II]/Hα has a constant value of 0.2 for the H II regions in positions 2 and 3, while its value changes from 0.2 to 0.6 along position 1 over the nucleus of the galaxy. This intensity ratio is plotted in Fig. 2(d). The higher value of [N II]/Hα in the nucleus is mainly due to an abundance effect, as will be discussed in Section 4.

3.2 Line intensities

Line intensities for all the identified emission lines have been measured in each spectrum using the program SPEED (kindly provided by Alex Schmidt), which integrates each line between selected limits and a fitted continuum. It can be seen in the spectra (Figs 5a, b and c) that the Balmer emission lines for most of the observed regions are affected by underlying absorption. We have corrected the emission lines by estimating the equivalent width of the absorption lines from the observed absorption profile. Errors have been estimated as the measured statistical noise of the continuum near the lines, multiplied by the FWHM of the line and divided by the intensity of the line. The observed line-intensities listed in Table 2 have been corrected for reddening according to the standard reddening curve (Whitford 1958) and assuming theoretical values for the Balmer decrement corresponding to case B recombination (Brocklehurst 1971). Due to the underlying absorption problem, we have used only the Hα/Hβ ratio to deduce the reddening constant C(Hβ), also given in Table 2. The agreement between the theoretical and reddening-corrected observed values for the ratio of Paschen lines to Hα indicates that underlying absorption and reddening have been properly corrected. The A_V does not vary significantly over the observed circumnuclear starburst regions, the largest extinction being observed at the bright nucleus $A_V = 1.13$. The Balmer extinction values obtained in this paper are lower than those found by GSK91.

In Table 2 we have also included the emission-line intensities of an extranuclear H II region (M), located at 30 arcsec N from the nucleus along slit position 1, in order to compare its physical properties with those of the circumnuclear regions. The continuum fluxes at 4000, 4678, 5510 and 8500 Å are listed in Table 3.

3.3 Gas densities and temperatures

Gas densities, obtained from the [S II]6717, 6731 Å line ratios (Osterbrock 1989), have been found to be of the order of 200 cm^{-3} for the H II regions and 8000 cm^{-3} for the nucleus. Four line ratios were used for temperature determination: [O III]4363/(5007 + 4959) Å, [O II](7320 + 7330)/3727 Å, [S III]6312/(9069 + 9532) Å and [S II](6717 + 6730)/(4068 + 4076) Å, following the relations proposed by Seaton (1975) and Aller (1984) with the atomic parameters given by Mendoza (1983). The derived values are listed in Table 4. Differences of temperature larger than 1000 K for different ions in each H II region are compatible with the flux errors of the weakest lines. We have adopted for the H II regions B, C and E the temperatures of [O II] and [O III] for low- and high-ionization zones respectively, because they
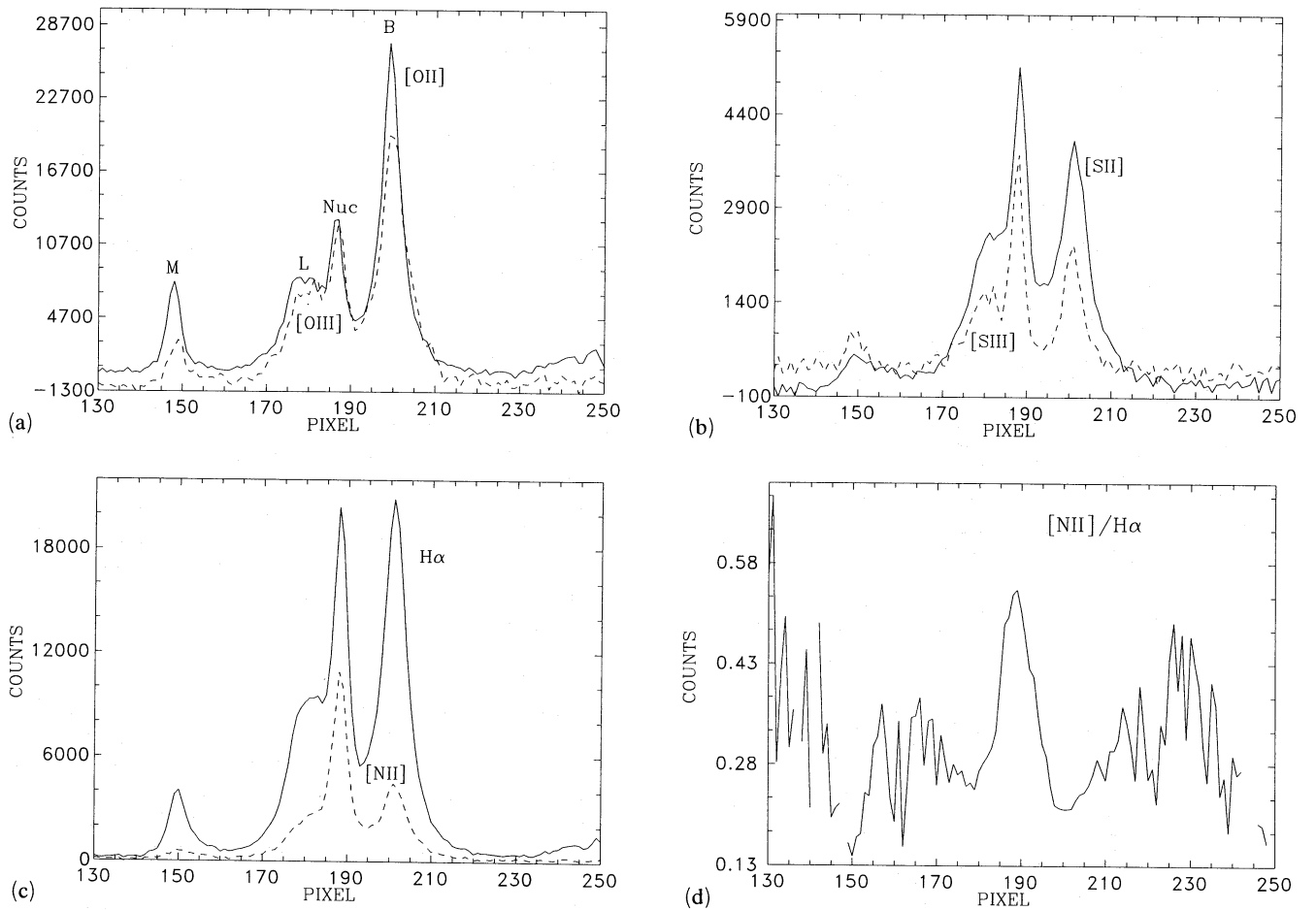
Figure 2. (a)–(c) Spatial profiles of the brightest emission lines through the nucleus and regions B and L; (d) [N II]/Hα. Notice that its value is considerably higher at the nucleus.

have lower errors. For the remaining regions, only one of two temperatures, t[O II] or t[O III], could be calculated directly, so we have estimated one from the other by means of Stasińska's (1982) relation:

$$t_{[O\,II]} = t_{[O\,III]} - 0.3(t_{[O\,III]} - 0.1).$$

The adopted values for the low- and high-ionization zones are listed in Table 4.

3.4　Ionic and total abundances

Ionic and total abundances for the most important elements He, O, N and S were calculated from their corresponding line-intensity ratios and the adopted electronic temperatures, following a three-level atom calculation using the atomic parameters given by Mendoza (1983). The estimated errors in the abundance determinations take into account the errors in the line fluxes and temperatures. We assumed that the total abundances of O, N and S are given by the following:

$$O/H = O^+/H^+ + O^{++}/H^+$$
$$N/H = N^+/H^+$$
$$S/H = S^+/H^+ + S^{++}/H^+.$$

The He/H$^+$ ratios are based on weighted means of the He I lines 4471, 5876 and 6678 Å for regions A, B, C and E. For

the nucleus and region L, only 5876 and 6678 Å have been used. The total abundance of helium has been computed from the derived value of He$^+$/H$^+$ corrected using the ionization correction factor (ICF) which takes into account the relative volumes of the He$^+$ and H$^+$ zones. The ICF has been estimated using the correlation between $R(He^+)/R(H^+)$ and [O III]/Hβ (Copetti, Pastoriza & Dottori 1986).

Ionic abundances of He$^+$/H$^+$, ICFs and total abundances of O, N and S are listed in Table 5.

4　H II REGION PARAMETERS

H II region emission-line spectra are controlled by three parameters, namely the shape of the ionizing spectrum, the ionization parameter (U) and the chemical composition of the gas. In order to analyse the behaviour of these parameters, we have computed simple H II region models using the photoionization code CLOUDY (Ferland 1989, improved version 1991, private communication).

Models assuming spherical symmetry, and uniform density and chemical composition, have been computed for ionizing stars of effective temperatures (T_{eff}) 3.5×10^4, 4.0×10^4 and 4.5×10^4 K, with spectral energy distributions taken from Mihalas' (1972) atmosphere models. Log U values used ranged from -1.0 to -3.0, as expected for low-metallicity regions (Evans & Dopita 1985). A particle
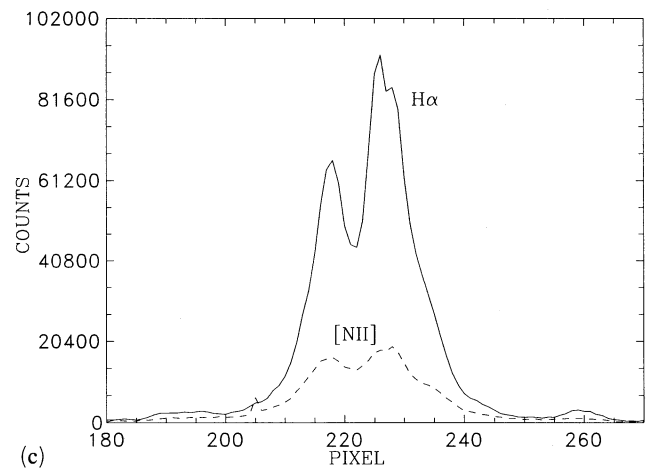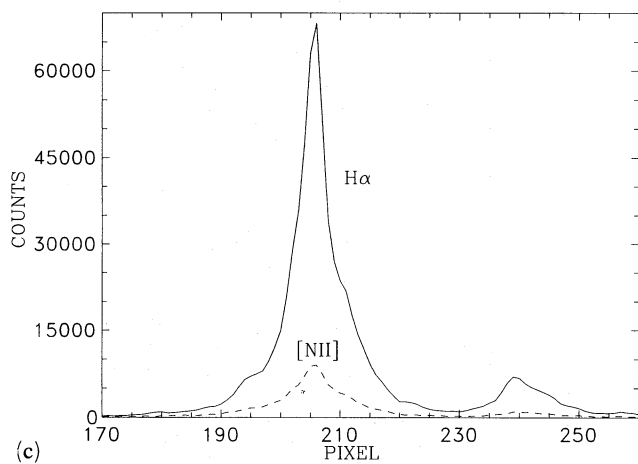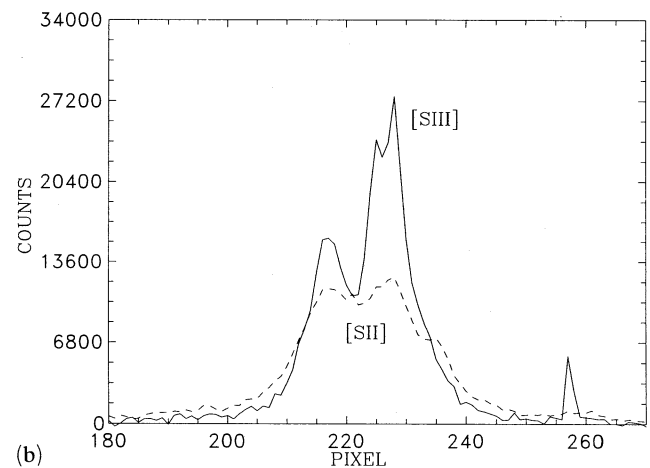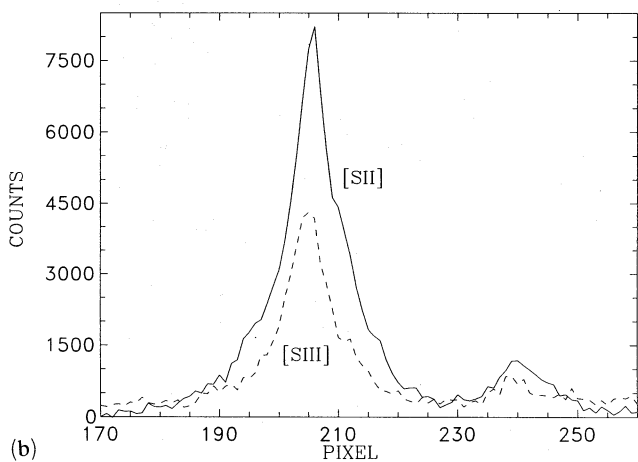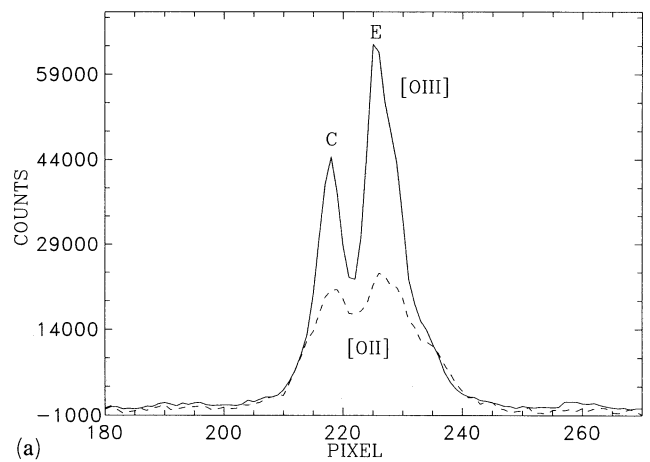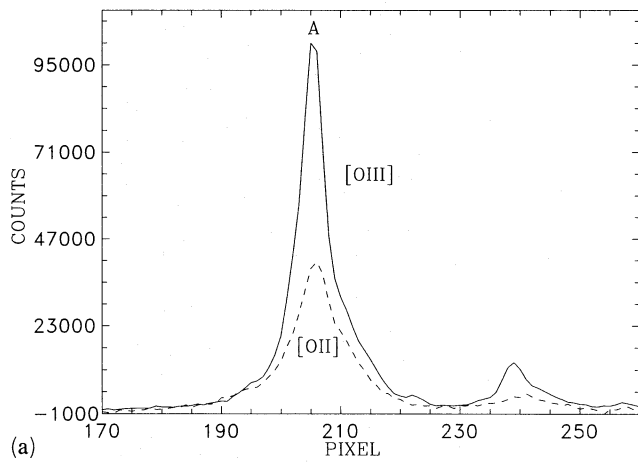
Figure 3. (a)–(c) Spatial profiles of the same emission lines as in Fig. 2, along region A.

Figure 4. (a)–(c) Spatial profiles of the same emission lines as in Fig. 2, for regions C and E.

density of 100 cm^{-3} (appropriate for the circumnuclear regions) and abundances $Z = 0.1$, 0.2, 0.4 and 0.8 Z$_\odot$ have been used to calculate the models.

Fig. 6(a) shows log([O III]/Hβ) versus log([S II]/Hα) for the computed models. The ratio [S II]/Hα is strongly dependent

on U (Evans & Dopita 1985), while [O III]/Hβ is sensitive to the T_{eff} of the ionizing stars and the metallicity of the gas. Fig. 6(b) shows the model trends for another good U indicator log([S II]/[S III]) as plotted against log([O III]/Hβ). Comparison with the H II region data indicates that values of log $U \sim -3$
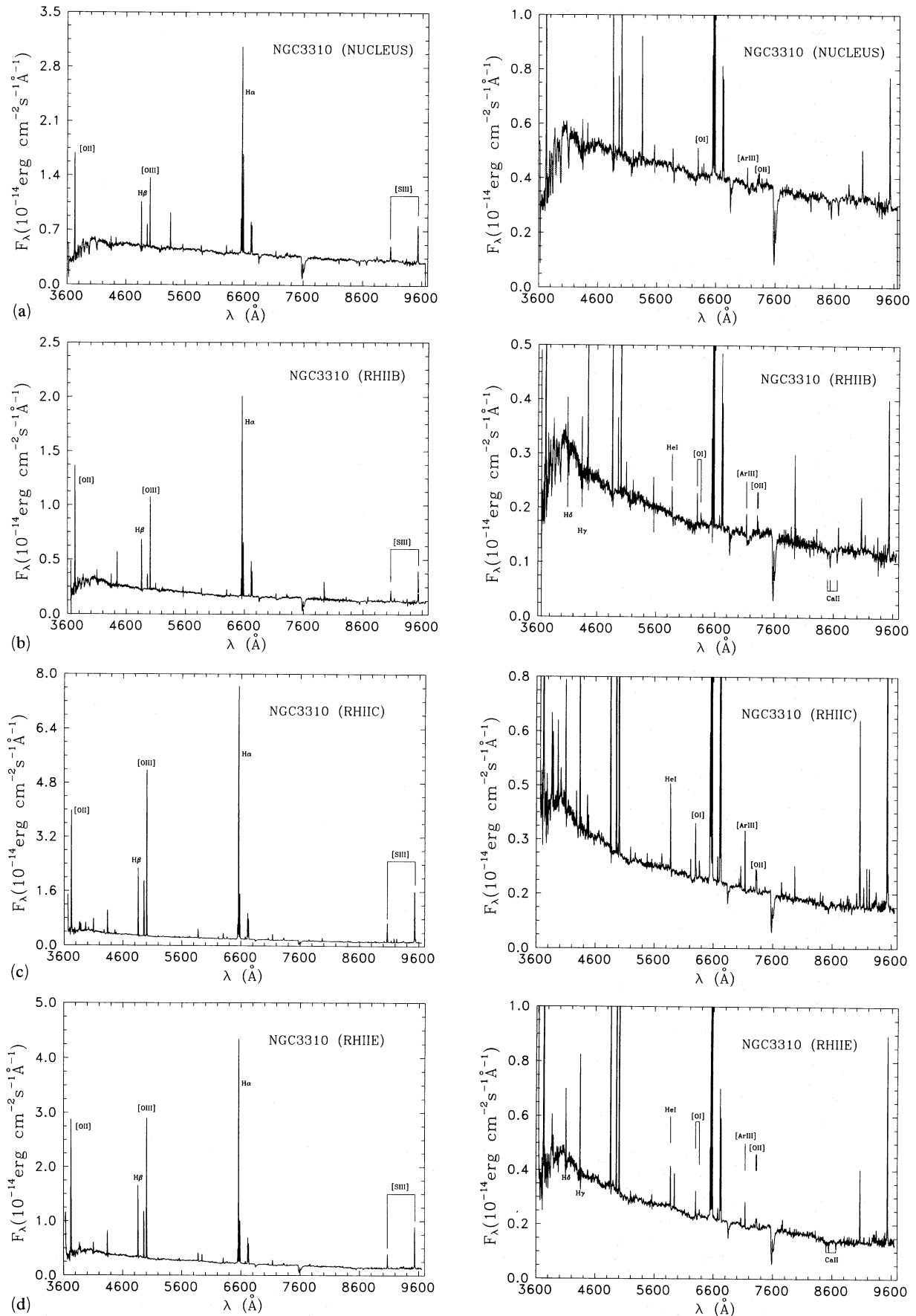
Figure 5. (a)–(f) Merged spectrum with two intensity scales for the nucleus and circumnuclear regions A, B, C, E and L. Notice the WR feature at 4600 Å. (g) An enlargement of the WR features due to WN4–5 stars in the Jumbo (A) region.
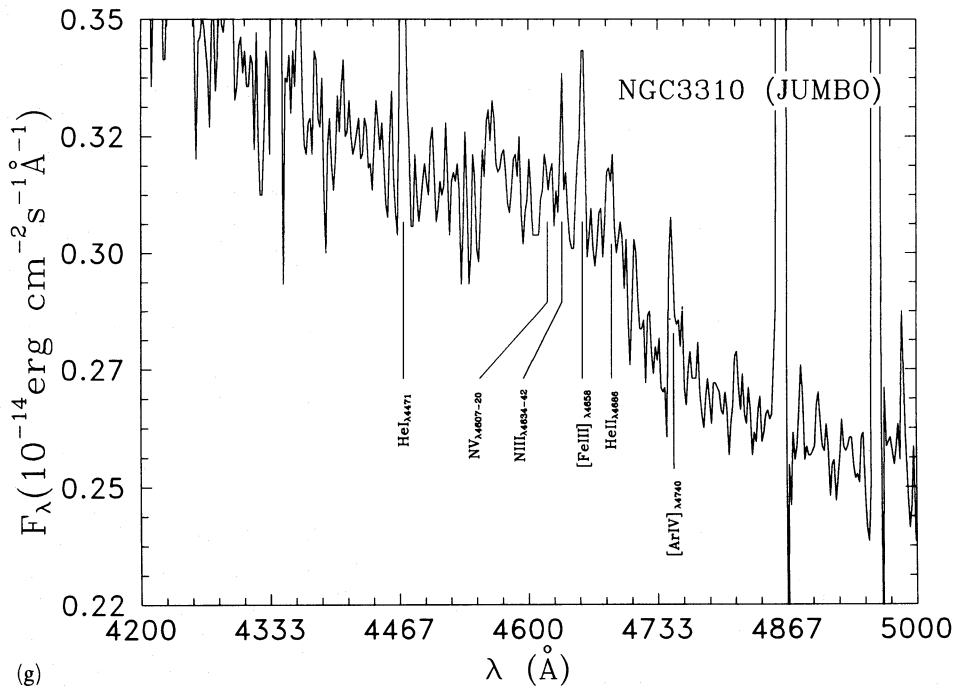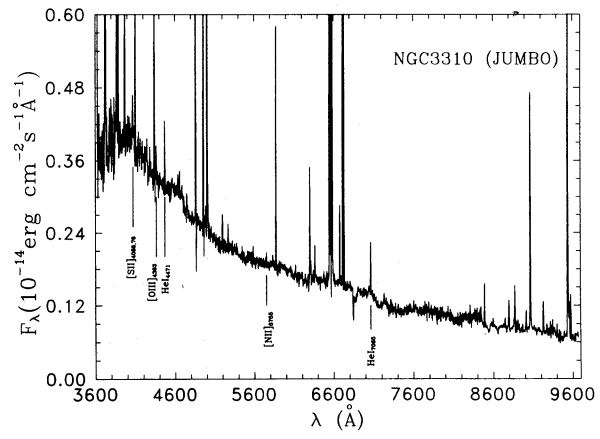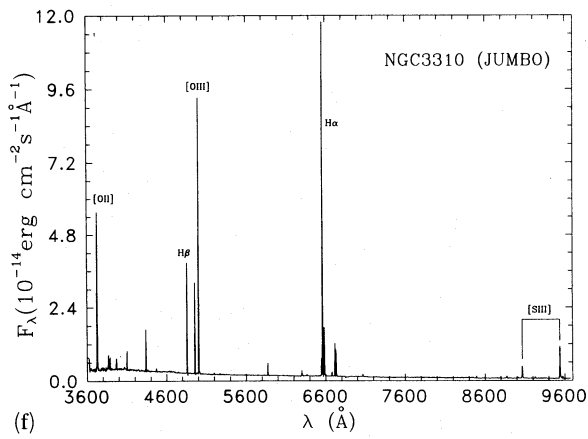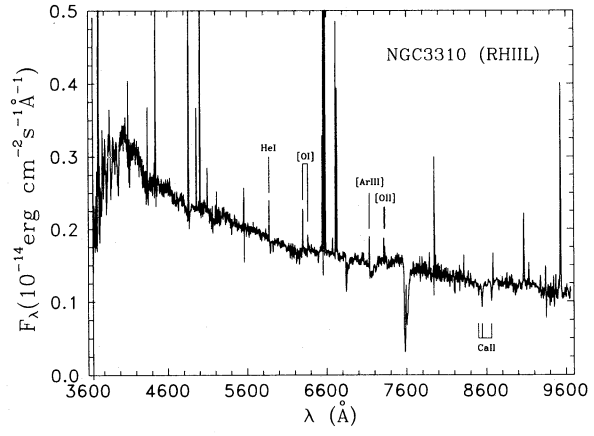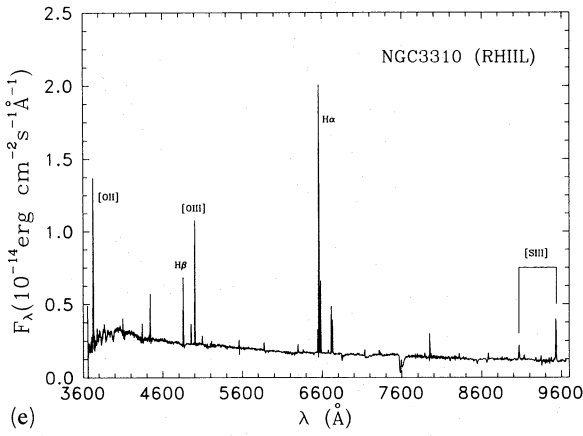
Figure 5 – *continued*

Table 2. Fluxes for the H II regions.

Region Line	Nuc	A	B	C	E	L	M
3727 [OII]	403±1	259±4	311±7	316±10	313±4.5	469±19	251±13
3869 [NeIII]	—	18±4	16±4	19±3	24±4.4	9.5±1	13
3889 H8, HeI	—	13±3.9	100±2	15±4	13±4.3	—	—
3967 [NeIII], Hε	—	17±5.3	9±2	16±3	—	—	—
4068,76[SII]	17±7	4.2±1.1	4:	4.4:	—	—	—
4101 Hδ	10±6	21:	21±1	25±2	19±4	22±0.4	33
4340 Hγ	29±9	39.5:	38±1	43±2	40±4	40±3	39
4363 [OIII]	—	1.8±0.5	2:	2.5±0.7	1.2:	—	—
4471 HeI	—	3.6±0.9	3:	3.3±1.2	3±1	—	—
4672 FeIII	—	16:	—	—	—	—	—
4861 Hβ	100±4	100±5.3	100±0.8	100±1	100±2.2	100±4	100
4959 [OIII]	43±4	74±0.7	59±1	81±1	69±0.1	57±4	91±20
5007 [OIII]	134±3	231±0.9	182±1	245±1.2	202±1.4	168±4	249±8
5012 HeI	—	1.5±0.6	—	—	—	—	—
5198 [NI]	8.6±3.6	1.5±0.3	3:	2.3±0.7	4±1	—	—
5270 [FeI]	—	0.9:	—	—	—	—	—
5755 [NII]	—	0.4:	—	—	—	—	—
5876 HeI	10±1	9.9±0.5	13±1	11±0.6	11±1.1	17±1	—
6300 [OI]	12±1	5.1±0.4	6±1	6.5±0.4	7±1	9.6±0.9	—
6312 [SIII]	—	1.1±0.3	—	1.4±0.2	1.4±0.7	1.1±0.5	—
6364 [OI]	23	1.4±0.5	2:	2.3±0.3	2.2±0.7	2.7±0.1	7
6548 [NII]	48.5±2	15±0.5	21±0.9	18±0.3	20±0.9	26±1.1	18
6563 Hα	290±2	288±0.4	287±0.9	288±0.4	287±1.2	289±1.6	287±5
6584 [NII]	146±2	46±0.3	66±1.1	55±0.4	59±0.7	79±1.3	43±10
6678 HeI	3±1	3.2±0.3	3±0.6	3.5±0.3	5±0.7	3.6±0.8	—
6717 [SII]	47±2	27±0.6	39±0.7	31±0.2	35±2	48±0.9	34±10
6730 [SII]	88±2	22±0.6	31±0.7	24±0.2	27±0.7	37±1.1	27±10
7065 HeI	—	—	1.9±0.6	2±0.2	1±0.7	—	—
7137 [ArIII]	5.7±1.1	0.7:	5±0.6	7.7±0.2	6.7±0.7	7.5±1.1	10
7319,30 [OII]	13±3	0.7:	7±1	5.5±0.5	6.6±0.7	6.3±2.1	8
7750 [ArIII]	.—	—	—	1.9±0.3	2.2:	—	—
8446 FeII	—	0.6	—	—	—	—	—
8598 P14	—	0.3	—	—	—	—	—
8750 P12	—	0.3	—	—	—	—	—
8863 P11	—	0.7	—	—	—	—	—
9015 P10	—	1	3±0.6	1.9±0.2	—	—	—
9069 [SIII]	23±1.3	12±0.4	22±0.7	24±0.6	22.2±1.6	18±1.2	21±10
9229 P9	—	1.5±0.3	2±0.7	5±0.6	—	—	—
9532 [SIII]	74±1.3	31±0.3	39±1	57±0.3	54±0.8	49±2.3	58±10
9556 P8	—	2.1±0.2	—	4.6±0.3	—	—	—
C(Hβ)	0.63	0.29	0.2	0.34	0.26	0.53	0.14
F(Hβ)	3.6	16.9	5.9	13.2	7.1	2.6	1.0
EW(Hβ) (Å)	12	73	29	55	30	15	38
L(Hβ)	2.7	5.7	1.6	5.0	2.3	1.5	0.2

Adopted distance = 12.5 Mpc; F(Hβ) in 10^{-14} erg cm^{-2} s^{-1}; L(Hβ) in 10^{39} erg s^{-1}.

Table 3. Continuum fluxes for the H II regions.

	Nuc	A	B	C	E	L	M
λ 4000	0.58	0.40	0.45	0.45	0.47	0.32	0.05
λ 4678	0.51	0.30	0.31	0.33	0.36	0.24	0.02
λ 5510	0.45	0.20	0.24	0.25	0.28	0.20	0.03
λ 8500	0.33	0.09	0.13	0.13	0.14	0.12	0.01

Fluxes in 10^{-14} erg cm^{-2} s^{-1}.

and $T_{eff} \sim 40\,000$ K are consistent in both diagrams. Using this U value, we have constructed abundance-dependent diagrams involving the strongest emission lines observed in the H II regions (Figs 6c and d). The continuous line in these diagrams connects models with equal abundance. The abundances of nitrogen and oxygen relative to solar, Fig. 6(c), show that the loci of the circumnuclear H II regions A, B, C, E and L, for log $U = -3$ and $T_{eff} \sim 4.0 \times 10^4$, fall

Table 4. Temperatures and densities for the H II regions.

	Nuc	A	B	C	E	L	M
x[SII]	0.82	0.02	0.02	0.02	0.01	0.01	0.02
t[OII]	0.62	—	1.10	0.98	1.08	0.70	0.97
t[OIII]	—	1.04	1.21	0.95	0.98	—	—
t[SIII]	—	1.24	—	1.04	1.10	1.06	—
t[SII]	0.43	1.34	—	1.18	—	—	—
t[NII]	—	0.78	—	—	—	—	—
T[I]	0.62	1.03	1.10±0.09	0.98±0.04	1.08±0.08	0.69±0.13	0.9
T[II]	—	1.04±0.1	1.21	0.95	0.98	0.69	0.9

Lines used to derive electron temperatures are listed in Section 3.3. Capital T values refer to the adopted temperatures for ions one (I) and two (II) times ionized used in the abundance analysis. t and x are temperature and electron density respectively, in units of 10^{-4}.

Table 5. Ionic and total abundances for the H II regions.

	Nuc	A	B	C	E	L	M
12+log O$^+$/H	8.32	7.97	7.97	8.1	7.99	8.39	8.0
12+log O^{++}/H	7.41	7.81	7.61	7.72	7.69	7.70	8.0
12+log O/H	9.0	8.21	8.13	8.25	8.17	8.47	8.3
Log O$^+$/N$^+$	1.26	1.05	0.93	1.08	0.99	1.15	1.1
12+log N/H	7.37	6.92	7.04	7.02	7.01	7.24	6.9
12+log S$^+$/H	6.32	5.40	5.53	5.41	5.49	5.70	5.5
12+log S^{++}/H	6.23	6.32	6.21	6.31	6.33	6.29	6.4
12+log S/H	6.57	6.37	6.29	6.37	6.39	6.39	6.4
(He$^+$/H$^+$) × 10^2	—	9.1	9.9	9.9	9.7	9.2	—
ICF	—	1.1	1.3	1.2	1.3	1.3	—

between the lines for $Z = 0.1$ and $Z = 0.2$ solar abundance. Models with higher log U and T_{eff} are shifted to the lower right of the diagram, far from any of the observed points. In the diagram log([S II] + [S III]/Hβ) versus log([O II] + [O III]/Hβ) (Fig. 6d), the points for the circumnuclear H II regions are shifted 0.2 dex to higher abundances.

The abundances, lower than 0.4 solar, obtained for the H II regions from the photoionization models, agree within the errors with the calculated values listed in Table 5.

For the nucleus, models with the same range of ionization parameters, effective temperature and metallicity, but a higher number density, have been calculated. The reddening-corrected line-intensity ratios of the nuclear spectra are best fitted by a model with $Z = Z_\odot$, $T_{eff} = 40\,000$ K, log U between -3.0 and -3.5 and $N_e = 8000$ cm^{-3}. The higher value of [N II]/Hα observed in the nucleus relative to the other regions is therefore not due to excitation but to metallicity.

5   THE WR FEATURES IN THE SPECTRUM OF REGION JUMBO

5.1   WR types

One striking feature of the blue spectrum of region A ('Jumbo') is a 200-Å wide bump, centred approximately at 4640 Å. This blend of emission lines is usually attributed to WR stars (Kunth & Sargent 1981: KS81; Osterbrock & Cohen 1982; Durret, Bergeron & Boksenberg 1985; Schild & Kunth 1986: SK86; Armus, Heckman & Miley 1988). In Fig. 5(g), the emission lines [Ar IV]4711 Å, He II 4686 Å,

[Fe III]4658 Å, N III 4634, 4641 Å and N V 4607, 4620 Å characteristic of this blend are identified. Some nebular lines are also present in this spectral region.

From the relative intensities of the WR emission lines in the blend, after removing the contribution from the nebular components, we can estimate the dominant spectral type of the WR population in the Jumbo region. The ratios of He II 4686 Å and [Fe III]4658 Å (nebular in origin) to N III 4634, 4641 Å are comparable to that in the spiral galaxy Mrk 710 (SK86). In both objects, the stellar lines present a narrow core, with the N III line comparable in intensity to the [Fe III] line, and both stronger than the He II one. We have fitted a core and an underlying broad component to the best-defined emission lines of stellar origin. Broad components are distinctive WR features (Smith & Kuhi 1981: SK81; Lundström & Stenholm 1984: LS84), while the narrow ones, clearly visible in our spectrum, are normally found in spectra of galaxies showing WR features (SK86). The broad component was assumed to be 1500 km s^{-1} wide for the He II 4686-Å line and 600–700 km s^{-1} for the N III 4634, 4641-Å and N V 4603 and 4620-Å lines as in KS81 for Tol3; this seems to reflect the real situation for a large number of WN stars in the SK81 and LS84 atlases.

From the analysis of the relative intensities of the WR emission lines, we conclude the following.

(i) The presence of N III and N V with almost the same intensity indicates WN4–5 as the most probable mean WR spectral type, while the absence of N III 4097 Å indicates a lack of earlier WN types.

(ii) Typical WC star features, like C III 5810 Å (van der Hucht et al. 1981), are not present. The narrow peak at 4658 Å is therefore attributed to [Fe III] and not to the C III–C IV 4650-Å line, which is very intense in WC stars. The absence of WC–WO stars is consistent with the low metallicity that we found for this region, since the lifetime of the WC–WO phase might be extremely short for $Z = 0.1$ Z$_\odot$ (Maeder 1990).

(iii) A blueward extension of the WR bump centred at 4560 Å and reaching up to the He I 4471-Å line is present. A similar feature but with different emission-line intensity distribution was detected in Mrk 499 by Campbell & Smith (1986).

5.2   The total number of WR and O stars in the Jumbo region

A rough estimate of the number of WR stars present in the Jumbo region can be obtained from the He II 4686-Å luminosity. The observed equivalent width and luminosity for He II and other WR lines are presented in Table 6. The luminosities have been calculated using a distance of 12.5 Mpc for the galaxy, deduced from the data in Bottinelli et al. (1984). The analysis in the previous section indicates that the dominant population of WR is of type WN4–5. These stars have $L_{WR}(4686) = 1 \times 10^{36}$ erg s^{-1} (SK86) and $M_B = -5$. To explain the observed He II luminosity in this region, therefore, as many as 220 WN4–5 are needed.

An upper limit for the number of O stars can be obtained by assuming that only they contribute to the hydrogen ionization. For the Jumbo region, the observed $L_{H\beta} = 4.39 \times 10^{39}$ erg s^{-1} gives a rate of Lyman ionizing

(c)

(d)

Figure 6 – *continued*

caveat is the higher spatial resolution of the 30 Dor observations. In our integrated spectra, we might be seeing WR stars that do not belong to the H II region.

6   MODELLING THE IONIZING ASSOCIATIONS

In order to obtain a better insight into the internal properties that govern the process of star formation in H II regions, we

have compared the observations with simple models of ionizing clusters. The models were computed using a code developed by R. Cid-Fernandes (Cid-Fernandes 1989; Cid Fernandes et al. 1992). The code uses the library of evolutionary tracks by Maeder & Meynet (1989) and Maeder (1990) (for stars between 0.8 and 120 $M_{\odot}$) and model atmospheres from Clegg & Middlemass (1987), Wesemael (1981) and Kurucz (1979).

Several observational constraints are used for the models.

Table 6. Equivalent width and luminosity of the WR feature.

	$\lambda(\text{Å})$	$W_{\text{neb}}(\text{Å})$	$W_s(\text{Å})$	$L(10^{38}\text{ erg s}^{-1})$
HeII	4686	1.2	3.9	2.2
NIII	4634-40	1.1	1.8	1.0
NV	4620	0.8	1.6	0.9
NV	4603	0.7	1.0	0.6
OII	4591	0.8	—	—
	[4550-4582]	—	3.1	—
[ArV]	4711	0.9	—	—
[FeIII]	4658	2.4	—	—
[ArV]	4625	0.7	—	—

W_{neb} and W_s correspond respectively to the equivalent widths of the nebular and star components of the line. Continuum at $\lambda 4686 = 4.8 \times 10^{-15}\text{ erg s}^{-1}$.

(i) The continuum colours. Observed continuum fluxes are listed in Table 3; four continuum points at 4000, 4680, 5500 and 8500 Å are included.

(ii) The luminosity and equivalent width of Hβ. These are listed in Table 2.

(iii) The detection of WR features, indicating the presence of evolved massive stars ($M \sim 40\text{ M}_\odot$).

(iv) The detection of a strong Ca II triplet at 8500 Å, indicating that red supergiant (RSG) stars are present (Terlevich et al. 1990). These RSG are associated with evolved intermediate-mass stars ($M < 20\text{ M}_\odot$).

(v) The observed equivalent width of the WR lines.

The equivalent width of the He II 4686 Å line observed in the Jumbo region is 3 Å. The observed value for WR4–5 stars ranges from 80 Å$\le W_{\text{WR}}(4686)\le 300$ Å (SK81). Thus, the contribution to the continuum at 4686 Å from stars other than the WR must be 25–100 times higher than that of the WR themselves.

We found that the observational constraints cannot be explained simultaneously with a stellar cluster having a single age. Regions A, B, C, E and L can be successfully modelled with two cycles of star formation:

(i) a population 15 Myr old providing the IR continuum and the IR Ca II triplet, and

(ii) a younger population providing the ionizing UV photons.

The cluster parameters (identified as I for the old cluster, II for the young cluster with WR and III for the young cluster without WR) and the derived fluxes for the selected continuum points are listed in Table 7 as well as the total ionizing photons $Q(\text{H})$ and $Q(\text{He})$ emitted by (1) all cluster stars, (2) only the WN stars, and (3) stars of $M > 20\text{ M}_\odot$. The properties are scaled to a 1-M$_\odot$ cluster.

The observed continuum slope, and the Hβ equivalent width and luminosity of the circumnuclear H II regions are well described by a model that has a large contribution (> 70 per cent) from the older stellar population (cluster I) and a small contribution from the younger one (cluster II). This is illustrated in Fig. 7.

To reproduce the spectral characteristics of region A requires a model with equal proportion of clusters I and II,

Table 7. Elements of the composite clusters.

	I	II	III
Age Myr	14.5	5.3	4.6
IMF M_{inf} ($M_\odot$)	1	1	1
IMF M_{sup} ($M_\odot$)	15	40	55
Slope	1.35	1.35	1.35
Total mass ($M_\odot$)	1	1	1
N stars	0.41	0.36	0.34
$Q(\text{H})$ (10^{43} photons s^{-1})	6.48	1559	2823
F_c ($\lambda 4000$)	5.49	28.59	62.78
F_c ($\lambda 4678$)	4.06	19.50	39.43
F_c ($\lambda 5510$)	3.23	12.12	23.44
F_c ($\lambda 8500$)	1.88	3.31	5.70
N WNs (10^{-4})	—	—	1.32
$Q(\text{H})$ (10^{45} photons s^{-1})	—	—	6.74
F_c ($\lambda 4000$)	—	—	1.31
F_c ($\lambda 4678$)	—	—	0.75
F_c ($\lambda 5510$)	—	—	0.42
F_c ($\lambda 8500$)	—	—	0.09
N $M > 20$ (10^{-3})	—	3.68	4.02
$Q(\text{H})$ (10^{46} photons s^{-1})	—	1.45	2.06
F_c ($\lambda 4000$)	—	5.36	12.44
F_c ($\lambda 4678$)	—	3.00	7.36
F_c ($\lambda 5510$)	—	1.67	4.26
F_c ($\lambda 8500$)	—	0.33	0.93

Fluxes in $10^{-13}\text{ erg cm}^{-2}\text{ s}^{-1}$.
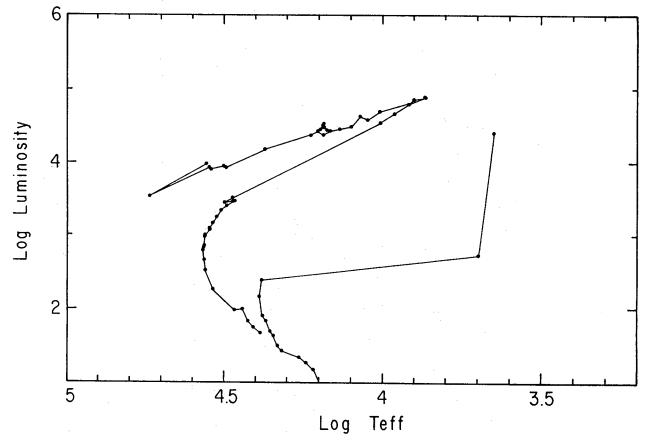
Figure 7. Synthesized two-bursts HR diagram for region A where WR stars are observed.

the last one providing the WR stars. Besides the relative contribution of both components, we can derive from the models the mass of the old and young components and the mass and number of ionizing stars and WN stars. These data are listed in Table 7 for the circumnuclear regions and in Table 8 for region A. Fig. 7 shows the HR diagram of the synthesized clusters for region A. Maeder's models require around 60 WN stars of 50–55 M$_\odot$ to account for the WR feature in this region. It is expected that stars up to 35–40 M$_\odot$ will go through WR phases for a region of such metallicity. The number of WN would then be increased by a factor of three, in agreement with the previous rough derivation of the number of WN4–5 contained in this region.

Table 8. Cluster mass of circumnuclear H II regions.

	Mass	B	C	E
Proportion	Cluster I	0.8	0.7	0.8
Proportion	Cluster II	0.2	0.3	0.2
	M_{old} ($10^6 M_\odot$)	1.0	1.0	1.2
	M_{young} ($10^4 M_\odot$)	6.8	7.5	7.8
	M_{is} ($M>20 M_\odot$)	2000	7000	3200
	N_{is} ($M=30 M_\odot$)	70	240	106

The penultimate row gives the total mass of ionizing stars with mass $\geq 20\ M_\odot$. The last row gives the total number of ionizing stars with mass $= 30\ M_\odot$.

Table 9. Cluster mass of region A.

	mass/$M_\odot$	N of stars
4.6 (Myr)	$3.1\ 10^5$	$1.1\ 10^5$
14.5 (Myr)	$7.0\ 10^5$	$2.7\ 10^5$
$12< M <40$	$5.9\ 10^4$	$3.1\ 10^3$
$29< M <40$	$1.3\ 10^4$	$4.0\ 10^2$
$50< M <55$ (WR)	$3.5\ 10^3$	59

The lower three rows give the mass intervals (in $M_\odot$) of the young component.

This simplified two-bursts scenario is not appropriate for the nucleus or region L, where the data are contaminated by the bulge light.

7 DISCUSSION AND CONCLUSIONS

The chemical composition of the gas has been obtained for the nucleus, four circumnuclear H II regions located inside a radius of 400 pc centred at the nucleus, the 'Jumbo' region at 600 pc south-west from the centre and the M region, which is located at 1600 pc north-west from the nucleus.

We found chemical abundances between 0.1 and 0.4 solar for the perinuclear, Jumbo and M H II regions. The nuclear abundance is about solar. For this range of metallicities, the diagram $\log([O\ III]/H\beta)$ versus $\log([S\ II]/H\alpha)$ is very sensitive to U and to the ionizing temperature. From this diagram, we have found $\log U = -3$ for all the observed H II regions (Fig 6a), the ionizing temperatures being in the range $37\,000 < T_{eff} < 40\,000$ K. The nuclear density is 8×10^3 cm^{-3}, much higher than that of the other H II regions, which show normal H II region values. The observed line ratios for the nucleus are best fitted by models with $\log U = -3.2$, $T_{eff} \sim 40\,000$ K and solar abundance.

Compared to other galaxies with circumnuclear H II regions (NGC 1097, 2903, 2950, 5236 and 5248, KKB) NGC 3310 presents two important characteristics: (i) the $L_{H\alpha}(\geq 4.0 \times 10^{39})$ of all the observed regions are among the brightest observed hotspots (see fig. 2 in KKB); region C is comparable to 30 Dor, and (ii) the metallicity in the perinuclear H II regions is notably smaller than that observed in other hotspot nuclei like NGC 1097, 1433, 7552, 1087 and 1408 ($12 + \log O/H \leq 8.95$ and $12 + \log N/H \leq 8.21$, Díaz 1985), which also have a Seyfert 2 or LINER nucleus.

We detected both WR and RSG (IR Ca II triplet) features in the spectrum of Jumbo, the most luminous of the observed

H II regions. The dominant WR types are WN4–5. The number of these stars is around 220 (60 Maeder's WN stars of 50–55 $M_\odot$ will produce the same result). Since theoretical models predict that only stars with masses lower than 60 $M_\odot$ can reach the RSG phase, the presence of WN and RSG in an H II region with strong emission lines suggests an extended activity of star formation lasting more than a few million years.

A two-age model – 5 and 15 Myr – for the starburst activity (equivalent to an extended star-formation activity) provides a good match to the observations. We also find that the emitted spectrum of the nucleus requires only photoionization by hot stars to be explained. The nuclear ionizing association (comparable to that in region L and five times smaller than that of the 'Jumbo' H II region) requires about 140 O6V stars to explain the observed nuclear ionizing flux.

REFERENCES

Aller L. H., 1984, Physics of Thermal Gaseous Nebulae. Reidel, Dordrecht
Armus L., Heckman T. M., Miley G. K., 1988, ApJ, 326, L45
Arp H., 1966, Atlas of peculiar galaxies. CalTech, Pasadena
Bertola F., Sharp N. A., 1984, MNRAS, 207, 47
Bottinelli L., Gouguenheim L., Paturel G., de Vaucouleurs G., 1984, A&A, 56, 381
Brocklehurst M., 1971, MNRAS, 153, 471
Campbell A. W., Smith L. J., 1986, in De Loore C. W. H., Willis A. J., Laskarides P., eds, Proc. IAU Symp. 116, Luminous Stars and Associations in Galaxies. Reidel, Dordrecht, p. 499.
Cid-Fernandes R., 1989, MSc. Thesis, IF-UFRGS, P. Alegre, Brazil
Cid-Fernandes R., Dottori H., Viegas S. M., Gruenwald R., 1992, in Edmunds M. G., Terlevich R., eds, 31st Herstmonceux Conference, Elements and the Cosmos. Cambridge University Press, Cambridge, p. 253
Clegg R. E. S., Middlemass D., 1987, MNRAS, 228, 759
Copetti M. V., Pastoriza M., Dottori H., 1986, A&A, 156, 111
de Vaucouleurs G., de Vaucouleurs A., Corwin H. H., 1976, Second Reference Catalogue of Bright Galaxies. University of Texas, Austin
Díaz A. I., 1985, PhD Thesis, University of Sussex
Díaz A. I., Pagel B. E. J., Wilson I. G., 1985, MNRAS, 212, 737
Durret F., Bergeron J., Boksenberg A., 1985, A&A, 143, 347
Evans I. N., Dopita M. A., 1985, ApJS, 57, 1
Ferland G., 1989, Internal Report 89-001. Astronomy Dept, Ohio State University
Grothues H. G., Schmidt-Kaler Th., 1991, A&A, 242, 357; GSK91
Heckman T. M., Balick B., 1980, A&A, 83, 100
Kennicutt R., Keel W., Blaha C., 1989, AJ, 97, 1022; KKB
Kunth D., Sargent W. L., 1981, A&A, 101, L1; KS81
Kurucz R. L., 1979, ApJS, 40, 1
Lundström I., Stenholm B., 1984, A&AS, 56, 43
Maeder A., 1990, A&AS, 84, 139
Maeder A., Meynet G., 1989, A&A, 210, 155

Melnick J., 1985, A&A, 153, 235

Mendoza C., 1983, in Flower D. R., ed., Proc. IAU Symp. 103, Planetary Nebulae. Reidel, Dordrecht, p. 143

Mihalas D., 1972, Tech. Notes/STR-76, National Center Atmosph. Research, Boulder, Colorado

Norman C., Scoville N., 1988, ApJ, 332, 124

Oke J. B., Gunn J. E., 1983, ApJ, 266, 713

Osterbrock D. E., 1989, Astrophysics of Gaseous Nebulae and Active Galactic Nuclei. University Science Books, Mill Valley, California

Osterbrock D. E., Cohen R. D., 1982, ApJ, 261, 64

Schild H., Kunth D., 1986, A&A, 169, 71; SK86

Seaquist E. R., Bignell R. C., 1977, A&A, 55, 163

Seaton M. J., 1975, MNRAS, 170, 475

Sersic J. L., Pastoriza M. G., 1967, PASP, 79, 152

Smith L. F., Kuhi L. V., 1981, Report 17, Joint Institute for Lab. Astrophys., Boulder, Colorado; SK81

Stasińska G., 1982, A&AS, 48, 299

Telesco C. M., Gatley I., 1984, ApJ, 284, 557

Terlevich E., Díaz A. I., Pastoriza M. G., Terlevich R., Dottori H., 1990, MNRAS, 242, 48P

Terlevich R., Melnick J., 1985, MNRAS, 213, 841

Terlevich R., Melnick J., Moles M., 1987, in Khachikyan E. Ye., Fricke K. J., Melnick J., eds, Observational Evidence for Activity in Galaxies. Reidel, Dordrecht, p. 499

van der Hucht K. A., Conti P., Lunström L., Stenholm B., 1981, Space Sci. Rev., 28, 227

van der Kruit P. C., 1976, A&A, 49, 161

van der Kruit P. C., de Bruyn A. G., 1976, A&A, 48, 373

Vorontsov-Velyaminov B. A., 1977, A&AS, 28, 1

Walborn N. R., 1991, in Haynes R., Milne D., eds, The Magellanic Clouds. Kluwer, Dordrecht, p. 145

Walborn N. R., Ebbets D. C., Parker J. W., Nichols-Bohlin J., White R. L., 1992, ApJ, in press

Wesemael F., 1981, ApJS, 45, 177

Whitford A. E., 1958, AJ, 63, 201